Optogenetic strategies for optimizing the performance of biosensors of membrane phospholipids in live cells

Yuanfa Yao[1, #,], Xiayan Lou[1, #], Guangwei Du[2, #], Luhong Jin[3], Jianxu, Li[4], Jingfang Liu[3], Yunyue Chen[3], Sunying Cheng[1], Tengjiao Zhao[1], Shuwei Ke[1], Luhao Zhang[3], Peng Zhang[4], Yingke Xu[3, 5*], Lian He[6, *], Hanbing Li[1, *]

1 Institute of Pharmacology, College of Pharmaceutical Science, Zhejiang University of Technology, Hangzhou, 310014, China

2 *Department of Integrative Biology and Pharmacology, University of Texas Health Science Center at Houston, Houston, TX 77030, USA.*

3 Department of Biomedical Engineering, Key Laboratory of Biomedical Engineering of Ministry of Education, State Key Laboratory of Modern Optical Instrumentation, Zhejiang Provincial Key Laboratory of Cardio-Cerebral Vascular Detection Technology and Medicinal Effectiveness Appraisal, Zhejiang University, Hangzhou, 310027, China

4 National Key Laboratory of Plant Molecular Genetics, Center for Excellence in Molecular Plant Sciences, Institute of Plant Physiology and Ecology, Shanghai Institutes for Biological Sciences, Chinese Academy of Sciences, Shanghai, 200031, China

5 *Department of Endocrinology, The Affiliated Sir Run Run Shaw Hospital, Zhejiang University School of Medicine, Hangzhou, 310016, China*

6 Department of Pharmacology, School of Medicine, Southern University of Science and Technology, Shenzhen, 518055, China.

# These authors contributed equally: Yuanfa Yao, Xiayan Lou, Guangwei Du;

*Correspondence should be addressed to **Drs. Hanbing Li**, **Lian He**, and **Prof. Yinek Xu**

Address for Dr. Hanbing Li (lead): Institute of Pharmacology, College of Pharmaceutical Science, 18 Chaowang Road, Zhejiang University of Technology, Hangzhou, 310014, China

Email: hanbing.li@163.com; Tel & Fax: +86-13185064285

Address for Dr. Lian He: Department of Pharmacology, School of Medicine, 1088 Xueyuan Avenue, Southern University of Science and Technology, Shenzhen, 518055, China.

Email: hel3@sustech.edu.cn; Tel & Fax:+86-0755-880100

Address for Prof. Yingke Xu: Department of Biomedical Engineering, 38 Zheda Road,

Yuquan Campus, Zhejiang University, Hangzhou, 310027, China

Email: yingkexu@zju.edu.cn ; Tel & Fax: +86-0571-87951091

Abstract

High-performance biosensors are crucial for elucidating the spatiotemporal regulatory roles and dynamics of membrane lipids, but there is a lack of improvement strategies for biosensors with low sensitivity and low-content substrates detection. Here we developed universal optogenetic strategies to improve a set of membrane biosensors by trapping them into specific region and further reducing the background signal, or by optically-controlled phase separation for membrane lipids detection and tracking. These improved biosensors were superior to typical tools and light simulation would enhance their detection performance and resolution, which might contribute to the design and optimization of other biosensors.

Introduction

Membrane lipids metabolism is a rapid spatiotemporal process and detecting their dynamics requires high-performance probes in live cells. Biosensors are essential for elucidating spatiotemporal regulatory roles of membrane lipids and have been extensively used to chase their changes in cells. A major optimization strategy for the improvement of biosensors is to alter their sensitivity to the targeted molecules by the regulation of the copies of the binding region or selection of appropriate binding motifs from various proteins of interest (POI). Contrast to in pursuit of improvement of biosensor sensitivity, it is a barely attempted aspect to improve their signal-to-noise ratio (SNR), especially for membrane phospholipids biosensor with limited sensitivity. It is undeniable that the unbound fraction of the overexpression of biosensors in cells has a greater or lesser impact on the detection performance, especially for some low-content tested substrates, which might require ‘washing out’ the dissociated biosensors and by which to improve the SNR.

How to remove the unbound biosensors to better image subcellular distribution of the

membrane lipids more clearly? A better approach to address this challenge might be to transport dissociative probes to specific uninterested region and minimize their impact on the SNR in cells. Trapping strategy based on optogenetics is supposed to provide solutions by anchoring or hiding the unbound probe to other unconcerned subcellular structures with photosensitive tool systems, such as LOVTRAP system[1] and LOV2-based nucleocytoplasmic transportation[2, 3]. Optogenetics has been widely used to regulate the spatiotemporal localization[4-7] and structural change of POI[8], and gene transcription[9-11], control the state of ion channel[12], as well as transport cell organelles[13, 14] in numerous studies. High temporal-spatial resolution and reversibility enable us to manipulate more sophisticated process and further understand mechanical principles of cellular physiological and pathological activities.

It is rarely reported that incorporation of optogenetics in biosensor development and improvement. To this end, our study harbored LOVTRAP system and LOV2 element to modify a set of membrane lipid biosensors. We trapped unbound biosensors into the cell nucleus or relocated them onto other uninterested structures under dark condition. Light stimulation liberated these stored probes, which is prepared for the binding to nascent phospholipids in response to agonists. While after treatment of inhibitors, the biosensor dissociated from membranes and then the fused optogenetic protein would transport these unbound molecules into the specific region in the dark for reduction of imaging interference. As expected, the reciprocation between the binding and dissociating process and optogenetics transportation of biosensors extremely reduced background noise and improved the SNR of biosensors. We used these approaches to improve the performance of phosphatidic acid (PA), and phosphatidylinositol (3,4,5)-trisphosphate (PIP3) biosensor. These optogenetics-based biosensors outperformed corresponding non-optimized biosensors. Moreover, to further improve the resolution of biosensors, we used CYR2/CIBN system to optically control the phase separation process of HOTag3 and HOTag6[15-17], and through which we significantly elevated the detection resolution of phosphatidylinositol 4-phosphate (PI4P) biosensor. This improved biosensor was also able to track PI4P dynamic at

plasma membrane. Collectively, the methodological improvements in this study might be referenced to design more high-performance biosensors and improve their detection resolution.

Results

Design of optogenetics-based biosensors with the LOVTRAP system

It has been shown that the optogenetics tool CRY2 might affect the behaviors of proteins that fused to its C-terminal, especially for short peptides[18]. We first tested whether this design was suitable for biosensor improvements. The PA biosensor was first reconstructed in light of the low basal level of PA in cells and the insensitivity of current PA biosensor, though Baskin group had developed an ingenious chemical strategy for labelling PA and indicating PLD activity[19-23]. After the linkage of the PA binding protein (PABP) (MDNCSGSRRRDRLHVKLKSLRNKIHKQLHPNCRFDD ATKTS) from yeast SPO20 protein to CRY2, this CRY2-based PA probe was mostly colocalized with exogeneously expressed PLD2 (**Fig. S1a-b**). However, the binding of the CRY2-based PA probe to PA dose not rely on light stimulation and our design has not improved the performance of PA biosensor either.

Due to the fact that most of PA biosensors in cells were unbound under basal state, we next considered the LOVTRAP system to trap these dissociative biosensors into specific region and released them for PA binding by light. To achieve this, we fused the Tom20 to the LOV2 domain and linked PABP to another effector ZDK1 (**Fig. 1a**). This version is called **Opto**genetics **PA** **S**uper **S**ensor based on **Z**DK/LOV2 (Opto-PASSz). In the dark, the combination of ZDK1 with LOV2 anchored most of unbound PA biosensors onto mitochondrial and reduced the background noise (**Fig. 1a-b**), which allowed us to observe the localization of PA probe on plasma membrane more clearly (**Fig. 1b**). The fluorescence intensity ratio of plasma membrane to the cytoplasm was used to assess the detection behavior of PA biosensors. The result indicated that this ratio was higher than the widely-used PA probe PASS-RFP[21, 23, 24] (**Fig. 1c**). The improved PA sensor Opto-PASSz were rapidly released from mitochondrial because of light-induced dissociation of ZDK1 with LOV2 (**Fig. 1d-e**).

The free Opto-PASSz probes were able to monitor the increase of intracellular PA (**Fig. 1d**, indicated in white rectangle). Although Opto-PASSz might only meet the demand for PA detection of plasma membrane, the result encouraged us to reduce the background noise by rational optogenetics design, which will facilite the enhancement of biosensor performance.

Design of optogenetics-based biosensors with circularly permuted LOV2 (cpLOV2)

To further improve the biosensors suitable for detecting PA at different subcellular structures, a LOV2-based nucleocytoplasmic transportation is proposed. The nucleus becomes amenable to store dissociative biosensors because the inner subunits of nucleus are membrane free except for nuclear envelope, and nucleocytoplasmic transportation using biosensors might be the optimal solution to improve the SNR and also meet the requirements for phospholipids imaging in the cytosol. Our previous work found that the position of some lipid probes, such as PA biosensor, at the N-terminal impaired the binding of the biosensor to PA (data not shown). Therefore, the cpLOV2 variant with the exclusive ability to fuse POI at the C-terminal, other than the wild type LOV2 domain, was preferentially selected as the optogenetics element for the modification of membrane lipid biosensors.

To this end, we selected seven the nuclear export sequences (NES) to fuse into the Jα helix at the N-terminal of cpLOV2 (**Fig. S1c**) and linked a fluorescin (eg. mCherry) and nuclear localization sequences (NLS: AAAKRSWSMAF) to its C-terminal (**Fig. S1c**). Under the dark condition, most of them resided in the cell nucleus (**Fig. S1d**). After blue light illumination, two of the seven tested NES exhibited an expected export of our primary design from the nucleus and the amino acid sequence (DEAAKELAGLDL) was strongest (**Fig. S1c-d**). Next, we compared the binding characters of PABP motif from different POI. The PABP from yeast Opi1p and Raf1 has defects in detecting PA levels at the plasma membrane (**Fig. S1e-i**). Thus we finally added the functional binding motif PABP from SPO20 to the C-terminal of cpLOV2 (**Fig. 2a**). The light-responsive transportation of Opto-PASSc between the

cytosol and the nucleus might affect the affinity to PA and thus we added one or more tandem copies of the PA binding region. This optogenetics-based PA biosensor was renamed **Opto**genetics **PA S**uper **S**ensor based on **c**pLOV2 (Opto-PASSc) (**Fig. 2a**).

Optogenetics-based biosensors displayed a high SNR in phospholipids imaging

The overexpression of Opto-PASSc in cells was substantially located in the nucleus (**Fig. 2b**). It indirectly reflected a low content of PA in the cytosol under the basal state. If the unconjugated PA biosensor was in the cytoplasm, its nonnegligible fraction might have an influence on imaging the real PA localization. In a small subset of transfected cells with a high level of PA, Opto-PASSc probe clearly labeled the plasma membrane (**Fig. 2b**) and were colocalized with PASS-RFP (**Fig. 2c**). In these cells, the background noise of Opto-PASSc was lower than PASS-RFP probe (**Fig. 2b-e**). Unexpectedly, the shuttle of Opto-PASSc probe between cytoplasm and the nuclear outlined the nuclear envelope (**Fig. 2f-g**), which suggested that the improved PA probe can detect the amount of PA on the nuclear envelope. Other sensors like PASS, PA probe derived from Opi1p, Raf1, and PDE4A1, were not equipped with this exclusive merit.

We then investigated whether blue light unwound the NES within the Jα helix of the cpLOV2 and then induced Opto-PASSc to enter into the cytosol. The fluorescence intensity ratio of cytoplasm to the nucleus was analyzed and this ratio increased in response to consecutive blue light illumination (**Fig. 2h**). However, light-induced nuclear export was not strong enough likely because another NES (NSNELALKLAG LDINKTE) between fluorescin and PA binding motifs. As non-polar amino acids such leucine and isoleucine are responsible for nuclear export via the interaction with nuclear pore complex, we then created two mutations (L5A and I14A) to inactivate the second NES action (**Fig. 2i**). The results of these mutations showed that the fluorescence intensity ratio of cytoplasm to the nucleus further reduced in the dark (**Fig. 2i-k**), which revalidated a low content of PA under non-stimulation condition. The improved Opto-PASSc was exported more after light stimulation (**Fig. 2l**). Since the above optogenetics improvements have exhibited an attractive ability to optimize

the traditional PA probe PASS, whether it is suitable for the enhancement of other membrane lipids biosensors? To this end, we replaced the PA binding motif with PH domain from BTK protein for PIP3 detection and renamed it as **Opto**genetics **PIP3 S**ensor based on **c**pLOV2 (Opto-PIP3Sc) (**Fig. S2a**). The result showed that PIP3Sc outperformed mCh-PH_{BTK} biosensor in detection of insulin-induced PIP3 increase (**Fig. S2a**).

Opto-PASSc outperformed PASS at PA labeling under different stimulations

In mammalians, Phospholipase Ds (PLDs) including PLD1, PLD2, and PLD6 are major enzymes that catalyze corresponding lipids such as phosphatidylcholine (PC) or cardiolipin (CL) into PA. However, the activation of PLD1 and PLD2 requires extra stimulation such as agonists of G-protein-coupled receptors and activation of PKC. We used an indirect activator PMA (a PKC activator) to increase PA level at the plasma membrane and assessed the performance of Opto-PASSc with different expression intensities in response to drug-induced PA increase in cells. Our results demonstrated that Opto-PASSc was superior to PASS-RFP in the chase of the PA dynamics at the plasma membrane regardless of expression level (**Fig. 3a-c**). The fluorescence intensity ratio of plasma membrane to the cytoplasm for Opto-PASSc was significantly higher than PASS-RFP in the vast majority of analyzed cells, and showed approximately 1.8-fold improvement of Opto-PASSc (**Fig. 3c**). In addition, we also found Opto-PASSc reflected more convincedly a high level of PA at plasma membrane in 293T in contrast to the typical PA probe PASS-RFP (**Fig. 3d-e**) and the result from biochemical assay also supported the above observation (**Fig. 3f**), which suggested the basal PLD activity might be associated with the cell types. This superiority of Opto-PASSc remained even we added one more copy of PABP into PASS-RFP (**Fig. S2k**).

It has been reported that the cellular PLD activity increased after starvation[25, 26]. As different PLD isoforms have preferential localization, for example, PLD1 preferentially resides at the cytosol and perinuclear, while PLD2 mainly localizes on the plasma membrane and PLD6 exclusively on mitochondrial, but it remains

unknown which PLD isoforms would be activated by starvation. We thereupon co-expressed PASS-RFP and Opto-PASSc into HeLa cells. Upon four-hour starvation in HEPES buffer, we observed that both PASS-RFP and Opto-PASSc were invariably colocalized at plasma membrane in most of observed cells (**Fig. 3g**). But Opto-PASSc clearly outlined an increase of PA with evidently higher fluorescence intensity ratio (**Fig. 3g-h**). Moreover, addition of PA binding motif copies also further improved the performance of Opto-PASSc (**Fig. 3h**). Unexpectedly, we found PASS-RFP and Opto-PASSc were colocalized on the endoplasmic reticulum (ER) in a small subset of starved cells (**Fig. 3g**). This phenotype is barely reported and not be elucidated in detail yet. We suspected that the elevatory PA level at ER might be related to biosynthesis of lipid droplets induced by starvation.

Given that PLD2 is mainly located at the plasma membrane, we observed the consistent results in PLD2-overexpressed cells. The optimal probes with different copies of PABP bound onto the plasma membrane, while they were reduced after inactivation of exogenous PLD2 by whether inactive mutation or chemical inhibitors (**Fig. S2b-j**). Collectively, we capitalized on Opto-PASSc to convincedly reveal a increased PA level at plasma membrane in response to starvation. This result was consistent with PA detection by the LC-MS method[26]. Although it has been demonstrated that PLD1 participated in the regulation of autophagy by the interaction with various molecules for PA production[25-27], our results that PA increases at the plasma membrane, to some extent, suggested the activation of PLD2 under starved stimulation. Other traditional methods such as biochemical regents Amplex™ Red Phospholipase D Assay Kit or lipidomics techniques (LC-MS etc.) might have difficulties in analyzing PLD isoform activity, expect for the PA bioimaging with such probe Opto-PASSc.

To further demonstrate whether the performance of Opto-PASSc relied on light-induced nuclear export, we compared the impact of the dark condition and consecutive blue light stimulation at the capture intervals on the detection ability of Opto-PASSc. Theoretically, light-mediated nuclear export would provide more

unbound probe for PMA-induced *de novo* synthesis of PA, which further enhanced fluorescence signal of the plasma membrane. To our expectation, the dissociative probes exported from the nucleus upon pulsing light stimulation at the capture interval (**Fig. 3i**, dotted blue line *v.s.* dotted gray line) and fluorescence intensity ratio (plasma membrane to the cytoplasm) was increased (**Fig. 3i**, solid green line *v.s.* solid gray line). In brief, our results suggested light illumination enhanced the detection performance of Opto-PASSc.

Establishment of optically-controlled phase separation for improvement of the detection resolution of biosensors

Biosensors with high-resolution might help to understand more specific mechanistic roles of membrane lipids in live cells. To improve the detection resolution, we first tried the SunTag system to detect lipids at single molecule resolution[28]. However, we found the formation of fluorescent clusters might only be controlled by chemical induction and fusion of the lipid binding motif with the SunTag element affected the affinity (data not shown). Besides, the spontaneous aggregation of single-chain variable fragment (scFv) antibody of GCN4 and huge size of expression system also discourage us to improve lipid biosensors. Therefore, to control the formation of fluorescent foci in cells, we capitalized on the interaction-sensitive phase separation of Homo-Oligomeric Tag3 (HOTag3)/HOTag6 system[15]. HOTag3 can be assembled into a hexamer and HOTag6 forms a tetramer. The phase separation would be triggered by the interaction of their fused fragment. By virtue of the light-responsive binding of the optogentic tool CRY2/CIBN, the phase separation process of HOTag3/HOTag6 system became controllable via light stimulation (**Fig. 4a**). Then we added lipid binding motif such as P4M domain from SidM to CIBN fragment for PI4P detection. In this way, the improved biosensor system would form fluorescent puncta in response to light and the combination of punctum-like probe with PI4P wound further enhance the detection resolution of P4M domain (**Fig. 4a**).

The results met the above expectations. We observed a 10-minute light pulse stimulation induced both green and red puncta in the cell (**Fig. 4b**). The fluorescence

intensity of these puncta was approximately 7.32-fold to the background (GFP channel) (**Fig. 4c**). Their plane size was approximately 0.240 μm^2 (**Fig. 4d**), which closed to the size of the SunTag foci. We then analyzed the kinestate of the phase separation spot on the plasma membrane, which might indicate the PI4P dynamic. It revealed the speed of most spots were approximately 133.6-210.2 nm/s (**Fig. 4e**). This value was less than energy-driven translocation of the kinesin (635-1 290 nm/s)[28]. Besides, we also noticed that a small subset of these spots displayed a limited range of motion (**Fig. S3a** and **Fig. 4f**) and the mechanistic elucidation of these nearly motionless spots were large unknown. To further assess the reversibility of light-induced phase separation, we cultured the stimulated cells in the dark for hours. It showed that a part of the phase separation puncta diffused without light illumination (**Fig. S3b** and **Fig. 4g**). As the disassociation time of CRY2 and CIBN is approximately 10-25 minutes, we concluded that diffusion time of phase separation puncta is mainly up to the disaggregation of HOTag3 and HOTag6.

Next, we investigated whether this technological improvement enhanced the detection resolution of PI4P biosensor. Our previous result indicated addition of one more copy of P4M domain extremely increased the affinity (**Fig. S3b**). Thus two copies of P4M were fused with CIBN-HOTag3 and we observed that phase separation puncta were located at the plasma membrane from both red and green channel after about 10-minute light stimulation in 293T and HeLa cells (**Fig. 4h**), which suggested evident improvement in detection resolution when compared to typical PI4P biosensors (**Fig. S3c-e**). More phase separation puncta were appeared at plasma membrane from TIRF microscopy (**Fig. 4i**). Furthermore, these puncta significantly reduced after treatment of an inhibitor of PI4P biosynthesis, phenylarsine oxide (PAO) for a half hour (**Fig. 4i**). The above results suggested that the biosensor based on the optically-controlled phase separation was enough sensitive to reflect the changes of membrane lipid and the high detection resolution enabled us to chase membrane lipids dynamic for understanding of more specific biological mechanisms.

Discussion

We previously reported and reviewed the important actions of PLDs and PA in cells[29-31], especially in cancer cells. However, to elaborate more biological actions of different PLD isoforms and to track their activities or dynamics, it requires detection approaches with higher performance. Baskin's group has developed an ingenious chemical detection platform based on click chemistry for PA labelling and tracking PLD activities according the transphosphatidylation of PLDs[19]. This advanced technique allowed us to analyze the distribution of activated PLDs in subcellular structure[20] and screen cells with high PLD activities[22]. Unlike such case, detecting other membrane lipids mainly relies on biosensors. They were developed by truncated binding motifs from specific proteins with a high affinity to membrane lipids. However, under the condition of single overexpression of these probes into cells, the unbound biosensors would influence the imaging process, especially for low-affinity probes and low-content substrate detection. Our engineering biosensors based on different optogeneitc systems has shown to reduce this interference by trapping the unbound molecules into targeted region. The system worked like a 'probe pool' and outputed dissociative probes for recognition of nascent membrane lipids after light stimulation. As expected, we reduced the background signal and increased the SNR, which eventually improved the performance of PA and PIP3 biosensors.

The light-responsive nucleocytoplasmic transportation of the improved biosensors had not only low background noise, but also met the demand for detection of membrane lipids in the cytoplasm subcellular organelles. It means that cpLOV2-based biosensors might be applied in more improved case of biosensors. However, we noticed that some lipids-binding motifs themselves had strong abilities of nuclear export or import owing to the presence of the internal NES or NLS-like amino acid sequence, which resulted in difficulties in the regulation of probe localization in basal state by addition of extra screening NES or NLS for reduction of the background signal. Therefore, the LOVTRAP-based improvement was an irreplaceable strategy in such condition. Except for this condition, the light-induced disassociation of LOV2 and ZDK1 was faster than the nuclear export of cpLOV2-based biosensor, which suggested that it

was suitable to track the rapidly-changed membrane lipid.

The typical membrane lipid biosensors are fused fluorescent protein for imaging. But most of fluorescent proteins were not appropriate molecules for resolution improvement by ultra-high resolution microscope such as stochastic optical reconstruction microscopy (STORM) and stimulated emission depletion microscopy (STED). Therefore, the current solution for the above difficulty is signal amplification by clustering dozens of fluorescent proteins, such as SunTag system. It has been widely used in tracking protein movements such as mRNA translation [32, 33]. In our study, we were encouraged by that whether spot-like phase separation was able to improve the detection resolution of biosensors. HOTag3 and HOTag6 were an ideal combination for controllable phase separation, which was screened by Shu's group[15]. They were sensitive to the interactions between their fused proteins. Our results suggested the HOTag3/HOTag6 punctum had similar size and dynamics in comparison with the SunTag system. Moreover, incorporation of optogenetic elements CRY2/CIBN with this technique allowed us to trigger the HOTag3/HOTag6-mediated phase separation more easily. Given that each phase separation punctum was armed with several lipid-binding motifs for grasping the membrane lipids, whether one phase separation spot indicated a single PI4P molecule was non-determined. But undeniably, this optically-controlled phase separation extremely enhanced the detection resolution of the improved PI4P biosensor. The bright puncta provided a possibility of tracking PI4P flow on the plasma membrane and also envisioned improvement of other metabolites detection in cells via the similar strategy.

In brief, our study first incorporated optogenetic strategies to optimize the performance of membrane biosensors. These optogenetics-based biosensors lowered the background signal and thus reflected phospholipids changes in cells more clearly. The optically-controlled phase separation was used to induced fluorescent spots and theses spots extremely increased the detection resolution of biosensors. The methodological improvements in this study might be referenced to design more high-performance and high-resolution biosensors, which contributes to understand

more spatio-temporal dynamics and regulatory roles of membrane lipids in live cells.

Acknowledgements

This research was supported by the National key research and development program (2021YFC2101001), the Cross Scientific Research Fund of Zhejiang University of Technology (2022JCY27) and the Natural Science Foundation of Zhejiang Province (LY18H070004).

Ethics declarations

The other authors declare no competing interests.

Contributions

Y.Y, X.L., L.H., and G.D. conceived the idea of optogenetic strategies for improvement of biosensors and discussed the optimization of opto-biosensors. H.L., L.H., Y.X., G.D., and P.Z. supervised the research. Y.Y, and X.L. designed and conducted most of the experiments. J.L., J.L., Y.C., S.C, T.Z., and S.K. prepared the samples. Y.Y, X.L., J.J. and L.Z. analyzed the experimental data and plotted figures. Y.Y, H.L., L.H., Y.X., and G.D. wrote and revised the paper with input from all authors.

References

1. Wang, H. et al. LOVTRAP: an optogenetic system for photoinduced protein dissociation. *Nature methods* **13**, 755-758 (2016).
2. He, L. et al. Circularly permuted LOV2 as a modular photoswitch for optogenetic engineering. *Nature Chemical Biology* **17**, 915-923 (2021).
3. Yumerefendi, H. et al. Light-induced nuclear export reveals rapid dynamics of epigenetic modifications. *Nature Chemical Biology* **12**, 399-401 (2016).
4. Strickland, D. et al. TULIPs: tunable, light-controlled interacting protein tags for cell biology. *Nature methods* **9**, 379-384 (2012).
5. Guntas, G. et al. Engineering an improved light-induced dimer (iLID) for controlling the localization and activity of signaling proteins. *Proceedings of the National Academy of Sciences* **112**, 112-117 (2015).
6. Liu, R. et al. Optogenetic control of RNA function and metabolism using engineered light-switchable RNA-binding proteins. *Nature Biotechnology* **40**, 779-786 (2022).
7. Kennedy, M.J. et al. Rapid blue-light–mediated induction of protein interactions in living cells. *Nature Methods* **7**, 973-975 (2010).
8. He, L. et al. Engineering of a bona fide light-operated calcium channel. *Nature Communications* **12**, 164 (2021).
9. Li, T. et al. A synthetic BRET-based optogenetic device for pulsatile transgene expression

enabling glucose homeostasis in mice. *Nature Communications* **12**, 615 (2021).

10. Zhou, Y. et al. A small and highly sensitive red/far-red optogenetic switch for applications in mammals. *Nature Biotechnology* **40**, 262-272 (2022).
11. Yu, Y. et al. Engineering a far-red light–activated split-Cas9 system for remote-controlled genome editing of internal organs and tumors. *Science Advances* **6**, eabb1777 (2020).
12. Deisseroth, K. & Hegemann, P. The form and function of channelrhodopsin. *Science* **357**, eaan5544 (2017).
13. Duan, L. et al. Optogenetic Control of Molecular Motors and Organelle Distributions in Cells. *Chemistry & Biology* **22**, 671-682 (2015).
14. van Bergeijk, P., Adrian, M., Hoogenraad, C.C. & Kapitein, L.C. Optogenetic control of organelle transport and positioning. *Nature* **518**, 111-114 (2015).
15. Zhang, Q. et al. Visualizing Dynamics of Cell Signaling In Vivo with a Phase Separation-Based Kinase Reporter. *Mol Cell* **69**, 334-346.e334 (2018).
16. Li, X., Combs, J.D., Salaita, K. & Shu, X. Polarized focal adhesion kinase activity within a focal adhesion during cell migration. *Nature Chemical Biology* (2023).
17. Li, X. et al. ATM-SPARK: A GFP phase separation–based activity reporter of ATM. *Science Advances* **9**, eade3760 (2023).
18. Tan, P. et al. Optical control of protein delivery and partitioning in the nucleolus. *Nucleic Acids Research* **50**, e69-e69 (2022).
19. Bumpus, T.W. & Baskin, J.M. Clickable substrate mimics enable imaging of phospholipase D activity. *ACS central science* **3**, 1070-1077 (2017).
20. Liang, D. et al. A real-time, click chemistry imaging approach reveals stimulus-specific subcellular locations of phospholipase D activity. *Proc Natl Acad Sci U S A* **116**, 15453-15462 (2019).
21. Tei, R. & Baskin, J.M. Spatiotemporal control of phosphatidic acid signaling with optogenetic, engineered phospholipase Ds. *Journal of Cell Biology* **219** (2020).
22. Bumpus, T.W., Huang, S., Tei, R. & Baskin, J.M. Click chemistry-enabled CRISPR screening reveals GSK3 as a regulator of PLD signaling. *Proc Natl Acad Sci U S A* **118** (2021).
23. Tei, R., Bagde, S.R., Fromme, J.C. & Baskin, J.M. Activity-based directed evolution of a membrane editor in mammalian cells. *Nature Chemistry* **15**, 1030-1039 (2023).
24. Zhang, F. et al. Temporal Production of the Signaling Lipid Phosphatidic Acid by Phospholipase D2 Determines the Output of Extracellular Signal-Regulated Kinase Signaling in Cancer Cells. *Molecular and Cellular Biology* **34**, 84-95 (2014).
25. Holland, P. et al. HS1BP3 negatively regulates autophagy by modulation of phosphatidic acid levels. *Nature Communications* **7**, 13889 (2016).
26. Dall'Armi, C. et al. The phospholipase D1 pathway modulates macroautophagy. *Nature Communications* **1**, 142 (2010).
27. Hussain, S.S. et al. RalA and PLD1 promote lipid droplet growth in response to nutrient withdrawal. *Cell Rep* **36**, 109451 (2021).
28. Tanenbaum, M.E., Gilbert, L.A., Qi, L.S., Weissman, J.S. & Vale, R.D. A protein-tagging system for signal amplification in gene expression and fluorescence imaging. *Cell* **159**, 635-646 (2014).
29. Yao, Y. et al. Novel function of biguanides in inhibition of phospholipase D1 expression via a translational mechanism in cancer cells. *Genes Dis* **10**, 1787-1790 (2023).

30. Yao, Y. et al. Structural insights into phospholipase D function. *Progress in Lipid Research* **81**, 101070 (2021).
31. Yao, Y. et al. Phospholipase D as a key modulator of cancer progression. *Biological Reviews* **95**, 911-935 (2020).
32. Wang, C., Han, B., Zhou, R. & Zhuang, X. Real-Time Imaging of Translation on Single mRNA Transcripts in Live Cells. *Cell* **165**, 990-1001 (2016).
33. Yan, X., Hoek, Tim A., Vale, Ronald D. & Tanenbaum, Marvin E. Dynamics of Translation of Single mRNA Molecules In Vivo. *Cell* **165**, 976-989 (2016).

Figure legends:

Figure 1: optimizing the biosensor of membrane phospholipids based on LOVTRAP system

a, the schematic diagram of the LOVTRAP-based optimal strategy for PA biosensor.

b, co-expression of Opto-PASSz with PASS-RFP in HeLa cells and **c**, quantitative analysis of the fluorescence intensity ratio of plasma membrane to the cytosol in GFP and RFP channel.

d, the representative images of Opto-PASSz probe distribution before and after blue light stimulation and **e**, quantitative analysis of the fluorescence intensity ratio of mitochondrial to the cytosol and plasma membrane to the cytosol, respectively.

Figure 2: the cpLOV-based optimal strategy for membrane phospholipids biosensors

a, the schematic diagram of the cpLOV-based optimal strategy for membrane phospholipids biosensors.

b, co-expression of Opto-PASSc with PASS-RFP in HeLa cells and **c**, colocalization analysis of Opto-PASSc and PASS-RFP.

d-e, comparison the background signal of Opto-PASSc with PASS-RFP.

f-g, Opto-PASSc was able to detect the PA level at the nuclear envelop.

h, the light-induced nuclear export of Opto-PASSc with two wild type NESs.

i-j, the background signal of Opto-PASSc after indicated NES mutation and **k**, quantitative analysis of the background signal of Opto-PASSc via the fluorescence intensity ratio of cytoplasm to the nucleus.

l, the light-induced nuclear export of Opto-PASSc with indicated NES mutation.

Figure 3: Opto-PASSc outperformed PASS at PA labeling under different stimulations

a, the detection performance of Opto-PASSc and PASS-RFP in response to PMA-induced PA increase and its quantitative analysis of the SNR of both probes (**b**).

c, quantitative analysis of the fluorescence intensity ratio of plasma membrane to the cytosol after 5 μM PMA treatment in HeLa cells with expression of Opto-PASSc and PASS-RFP.

d, Opto-PASSc clearly labelled PA at plasma membrane and its analysis (**e**) of the fluorescence intensity ratio of plasma membrane to the cytoplasm in 293T cells under basal state.

f, the chemical assay compared the basal PLD activities between HeLa and 293T cells.

g, the PA detection of Opto-PASSc and PASS-RFP in HeLa cells after four-hour starvation in HEPES buffer and **h**, quantitative analysis of the the fluorescence intensity ratio of plasma membrane to the cytoplasm for Opto-PASSc with different copies of PABP motifs.

i, blue light illumination enhanced the performance of Opto-PASSc in response to PMA stimulation.

Figure 4: improvement of biosensors based on the optically-controlled phase separation

a, the schematic diagram of the optically-controlled phase separation for optimizing membrane phospholipids biosensors.

b, the light-induced binding of CRY2/CIBN triggered the phase separation via HOTag3/HOTag6.

c, the brightness of phase separation puncta and their sizes (**d**).

e, the speeds of phase separation puncta on the plasma membrane and **f**, tracking of the representative spot movements.

g, insoluble the phase separation puncta slowly disaggregated under dark condition.

h, improvement of the detection resolution of the biosensor based on the

optically-controlled phase separation.

i, the improve probe chased the reduction of PI4P on the plasma membrane in response to PAO (30 μM)treatment.

Supplementary figure 1: Optogenetic strategies based on different optogenetic elements for optimizing PA biosensors

The colocalization of GFP-PLD2 and the CRY2-based PA biosensor with one (**a**) or two (**b**) copies of PABP motif from SPO20.

c, the design of cpLOV-based nucleocytoplasmic transportation and **d**, representative images of cpLOV-mCh-NLS distribution in cells under non-stimulation condition and quantitative analysis of the light-induced nuclear export of cpLOV-mCh-NLS with fusion of different NES sequences.

e, the schematic diagram of the cpLOV-based PA biosensor (Opto-PASSc) with two PABP motifs from yeast Opi1p and representative images of co-expression of Opto-PASSc with PASS-RFP or mCh-PLD2 in HeLa cells (**f**) and in 293T cells (**g**).

h, the schematic diagram of the cpLOV-based PA biosensor (Opto-PASSc) with three PABP motifs from Raf1 protein and representative images of its co-expression with mCh-PLD2 (**i**).

Supplementary figure 2: comparison of the detection behaviors of Opto-PIP3Sc, Opto-PASSc with corresponding typical probes

a, the schematic diagram of the cpLOV-based PIP3 biosensor and its detection behavior after insulin treatment.

b-**i**, the PA detection by Opto-PASSc with indicated copies of PABP motifs and PASS-RFP in the PLD2-overexpressed (PLD2 wild type or inactive mutation) and **j**, co-expression of PLD2 (WT) and Opto-PASSc in HeLa cells after FIPI treatment.

k, representative images and analysis of the detection performance of Opto-PASSc and PASS-RFP with same copy of PABP motifs.

Supplementary figure 3: the optically-controlled phase separation improved the detection resolution of PI4P biosensor

a, the representative image of the phase separation foci on the plasma membrane.

b, the representative image of the phase separation foci from the red channel (mCh-CRY2-HOTag6) under indicated treatments.

c, the optically-controlled phase separation improved the detection resolution of PI4P biosensor at the plasma membrane in HeLa cells and its analysis (**d**)

e, the representative image of the typical PI4P biosensors with one or two copies of P4M motifs.

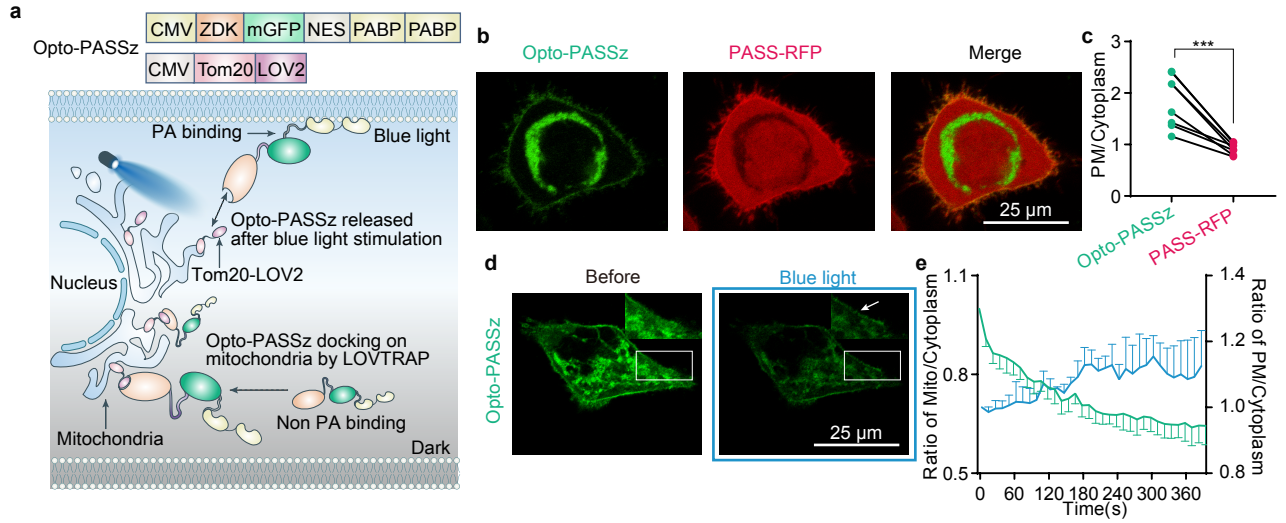
a
Opto-PASSz
CMV
ZDK
mGFP
NES
PABP
PABP
CMV
Tom20
LOV2
PA binding
Blue light
Opto-PASSz released after blue light stimulation
Tom20-LOV2
Nucleus
Opto-PASSz docking on mitochondria by LOVTRAP
Non PA binding
Mitochondria
Dark
b
Opto-PASSz
PASS-RFP
Merge
25 μm
c
PM/Cytoplasm
***
Opto-PASSz
PASS-RFP
d
Before
Blue light
Opto-PASSz
25 μm
e
Ratio of Mito/Cytoplasm
Ratio of PM/Cytoplasm
Time(s)

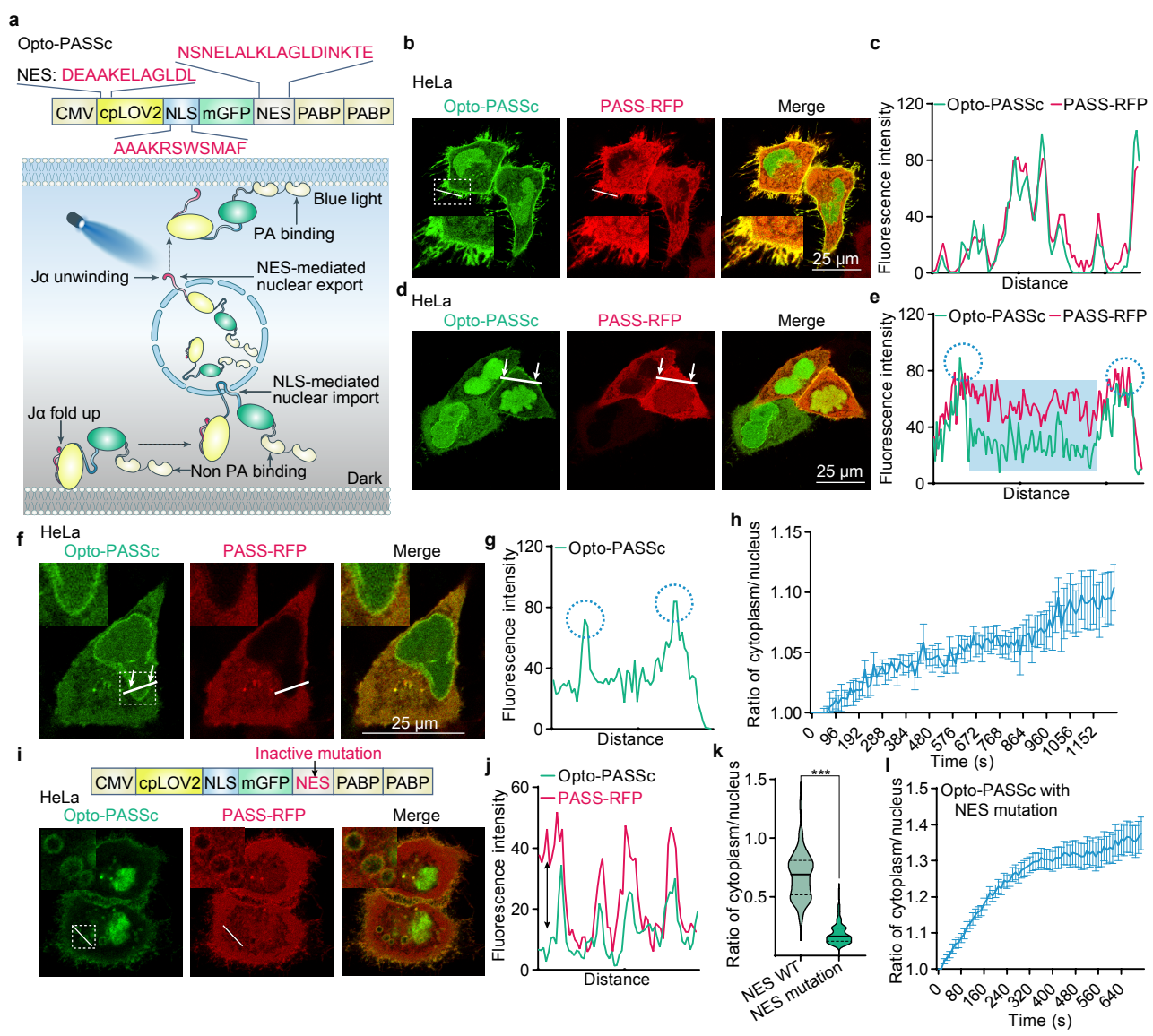
a
Opto-PASSc
NSNELALKLAGLDINKTE
NES: DEAAKELAGLDL
CMV
cpLOV2
NLS
mGFP
NES
PABP
PABP
AAAKRSWSMAF
Blue light
PA binding
Jα unwinding
NES-mediated nuclear export
NLS-mediated nuclear import
Jα fold up
Non PA binding
Dark
b
HeLa
Opto-PASSc
PASS-RFP
Merge
25 μm
c
Opto-PASSc
PASS-RFP
Fluorescence intensity
Distance
d
HeLa
Opto-PASSc
PASS-RFP
Merge
25 μm
e
Opto-PASSc
PASS-RFP
Fluorescence intensity
Distance
f
HeLa
Opto-PASSc
PASS-RFP
Merge
25 μm
g
Opto-PASSc
Fluorescence intensity
Distance
h
Ratio of cytoplasm/nucleus
Time (s)
i
Inactive mutation
CMV
cpLOV2
NLS
mGFP
NES
PABP
PABP
HeLa
Opto-PASSc
PASS-RFP
Merge
j
Opto-PASSc
PASS-RFP
Fluorescence intensity
Distance
k
***
Ratio of cytoplasm/nucleus
NES WT
NES mutation
l
Opto-PASSc with NES mutation
Ratio of cytoplasm/nucleus
Time (s)

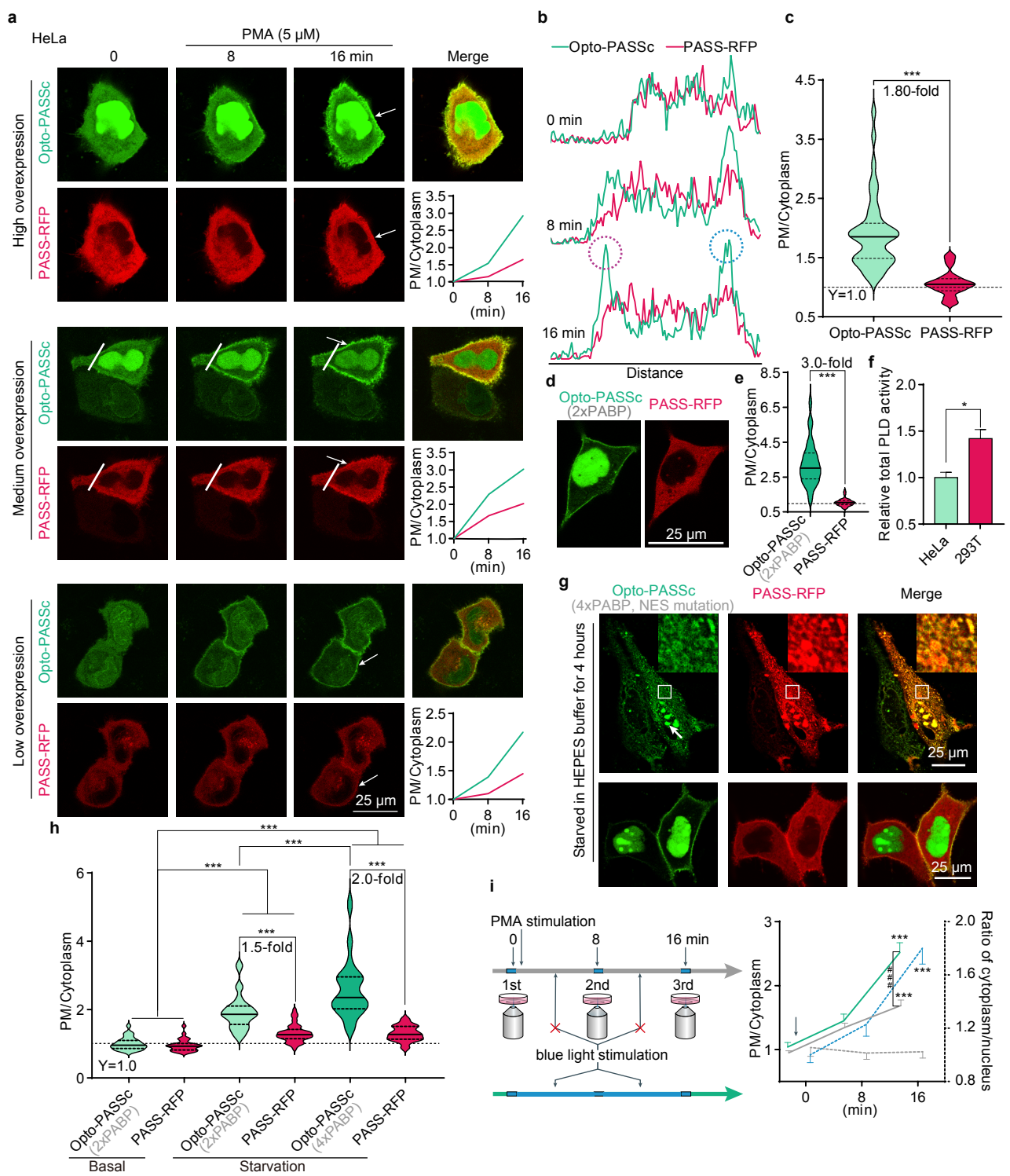
a
HeLa
PMA (5 μM)
0
8
16 min
Merge
High overexpression
Opto-PASSc
PASS-RFP
PM/Cytoplasm
(min)
Medium overexpression
Low overexpression
25 μm
b
Opto-PASSc
PASS-RFP
0 min
8 min
16 min
Distance
c
1.80-fold
Y=1.0
Opto-PASSc
PASS-RFP
d
Opto-PASSc (2xPABP)
PASS-RFP
25 μm
e
3.0-fold
f
Relative total PLD activity
HeLa
293T
g
Opto-PASSc (4xPABP, NES mutation)
PASS-RFP
Merge
Starved in HEPES buffer for 4 hours
25 μm
h
2.0-fold
1.5-fold
Y=1.0
Basal
Starvation
i
PMA stimulation
1st
2nd
3rd
blue light stimulation
Ratio of cytoplasm/nucleus

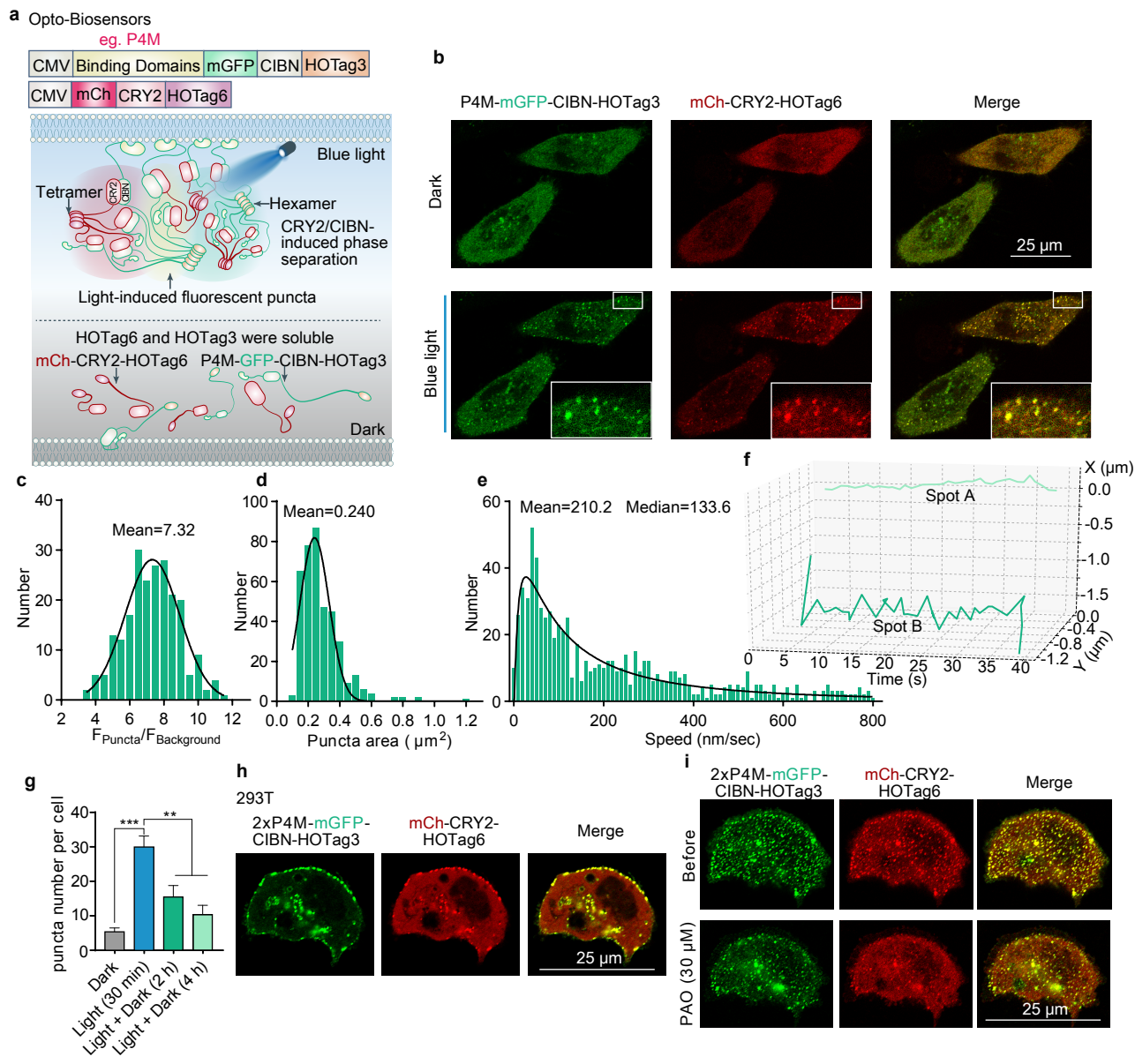
a
Opto-Biosensors
eg. P4M
CMV
Binding Domains
mGFP
CIBN
HOTag3
CMV
mCh
CRY2
HOTag6
Blue light
Tetramer
CRY2
CIBN
Hexamer
CRY2/CIBN-induced phase separation
Light-induced fluorescent puncta
HOTag6 and HOTag3 were soluble
mCh-CRY2-HOTag6
P4M-GFP-CIBN-HOTag3
Dark
b
P4M-mGFP-CIBN-HOTag3
mCh-CRY2-HOTag6
Merge
Dark
Blue light
25 μm
c
Mean=7.32
Number
F_Puncta/F_Background
d
Mean=0.240
Number
Puncta area (μm²)
e
Mean=210.2
Median=133.6
Number
Speed (nm/sec)
f
Spot A
Spot B
X (μm)
Y (μm)
Time (s)
g
puncta number per cell
***
**
Dark
Light (30 min)
Light + Dark (2 h)
Light + Dark (4 h)
h
293T
2xP4M-mGFP-CIBN-HOTag3
mCh-CRY2-HOTag6
Merge
25 μm
i
2xP4M-mGFP-CIBN-HOTag3
mCh-CRY2-HOTag6
Merge
Before
PAO (30 μM)
25 μm